Article

An Unsupervised Error Detection Methodology for Detecting Mislabels in Healthcare Analytics

Pei-Yuan Zhou * , Faith Lum , Tony Jiecao Wang , Chen Dan , San Lee , Andrew K.C. Wong

Posted Date: 4 July 2024

doi: 10.20944/preprints202407.0425.v1

Keywords: Unsupervised Learning; Error detection; Pattern Discovery and Disentanglement; Healthcare Data Analysis

Preprints.org (www.preprints.org) | NOT PEER-REVIEWED | Posted: 4 July 2024 doi:10.20944/preprints202407.0425.v1

Article

An Unsupervised Error Detection Methodology for Detecting Mislabels in Healthcare Analysis

Peiyuan Zhou [1,*], Faith Lum [1], Tony Jiecao Wang [1], Chen Dan [2], San Lee [2] and Andrew K.C. Wong [1]

[1] University of Waterloo, Waterloo, Canada; faith.lum@uwaterloo.ca (F.L.); jiecao.wang@uwaterloo.ca (T.J.W.); akcwong@uwaterloo.ca (A.K.C.W.)

[2] SpassMed Inc., Toronto, Canada; chen.dan@spassmed.ca (C.D.); sanlee@spassmed.ca (S.L.)

[*] Correspondence: p44zhou@uwaterloo.ca

Abstract: Medical datasets may be imbalanced and contain errors due to subjective test results and clinical variability. The poor quality of original data affects classification accuracy and reliability. Hence, detecting abnormal samples in the dataset can help clinicians make better decisions. In this study, we propose an unsupervised error detection method using patterns discovered by the Pattern Discovery and Disentanglement (PDD) model, developed in our earlier work. Applied to the large data, the eICU Collaborative Research Database for sepsis risk assessment, the proposed algorithm can effectively discover statistically significant association patterns, generate an interpretable knowledge base for interpretability, cluster samples in an unsupervised learning manner, and detect abnormal samples from the dataset. As shown in the experimental result, our method outperformed K-Means by 38% on the full dataset and 47% on the reduced dataset for unsupervised clustering. Multiple supervised classifiers improve accuracy by an average of 4% after removing abnormal samples by the proposed error detection approach. Therefore, the proposed algorithm provides a robust and practical solution for unsupervised clustering and error detection in healthcare data.

Keywords: unsupervised learning; error detection; pattern discovery and disentanglement; healthcare data analysis

1. Introduction

Machine Learning (ML) models are used to process big healthcare datasets, and various ML models have proven effectiveness for predictive analytics and diagnostic applications [1]. For instance, Alvin et al. [2] demonstrates how deep learning models improve healthcare quality when applied to electronic health records (EHR) data. However, there are several challenges that machine learning may face in healthcare data analysis[3].

First, machine learning models always require accurate and complete datasets to ensure effective functionality. Thus, data quality significantly influences reliability and can impact clinical decision-making and patient care [4]. Specifically, the reliability of labels in healthcare data is crucial for the effectiveness of predictive models. When class labels are inaccurate or unreliable, even models with high predictive accuracy may not be reliable due to their dependence on incorrectly labelled data. Moreover, it is difficult for medical experts to manually detect these elusive errors due to lack of contextual information, limiting data privacy regulations, and the sheer scale of data to be reviewed [5].

Next, healthcare providers often need clear explanations for AI-driven decisions, which is challenging with complex models like deep neural networks. Many of these models are black box models, lacking transparency and accountability, which can lead to severe consequences [6]. For high-stake applications such as healthcare, the judicial system, and human resource recruitment, machine learning models should be transparent to allow for interpreting their predictions and explaining decision boundaries [7] [6] [8]. As suggested by Rudin [6], creating an interpretable model is a better solution than trying to explain black box models. This allows for synergistic improvement as the interpretable model both integrates and enhances expert knowledge.

Finally, many medical conditions are rare, resulting in imbalanced datasets where the number of cases for one outcome is much smaller than those for others. This class imbalance problem [9] has posed a challenge for years, with machine learning models still struggling to overcome it.

To address these challenges, we have developed a model based on statistical theory, named Pattern Discovery and Disentanglement (PDD) [10] [11], to efficiently discover compact sets of significant association patterns linked to their primary sources. It generates a knowledge base interlinking patterns, entities, and sources for visualization, interpretation, and further exploration. In this paper, we propose an unsupervised error detection method using patterns discovered by the PDD to improve the quality of the data.

To identify errors, existing error correction strategies often rely on prediction results from a trained model. These strategies include those implemented through Cleanlab, isolation forest, and AdaBoost. Cleanlab's system [12] can provide model-specific insights, which are highly dependent on the model's quality and may inherit biases. Isolation Forest can be used for anomaly detection by determining which points require fewer partitions to separate from other data points [13]. AdaBoost calculates the weighted error of the classifier for each iteration, giving higher weights to misclassified samples to emphasize their importance in the next iteration [14]. Unlike the above strategies, our proposed error detection approach does not depend on a specific model and avoids the issue of model bias. Moreover, it provides an interpretable explanation of dataset and error properties, ensuring a higher-quality dataset before any model training occurs.

To demonstrate the effectiveness of the proposed algorithm, we applied it to the eICU Collaborative Research Database (eICU-CRD) [15] for assessing sepsis risk based on vital signs. Sepsis is a condition that requires prompt diagnosis [16]. Our analysis confirms that the algorithm successfully addresses imbalances in healthcare data, identifies errors and mislabels, and enhances sepsis detection.

Therefore, the contributions of this paper are significant both algorithmically and practically. Algorithmically, 1) we introduce an unsupervised algorithm that effectively discovers patterns or groups of patterns associated with distinct classes, which are functional and statistically independent from the patterns of other classes, as demonstrated by our experimental results; and 2) we propose an error detection method to detect mislabels in the dataset, the effectiveness of which is validated through comparing classification results before and after error correction. Practically, 1) the application of our algorithm to the disease sepsis reveals insightful characteristics of patients and patient groups, enhancing our understanding of the disease's impact; and 2) the error detection process improves the quality of the dataset, helping to identify outliers or mislabelled patient records.

2. Materials and Methods

2.1. Dataset and Preprocessing

The eICU-CRD [15] includes data from critical care unit patients across the United States for 2014 and 2015. We used the same dataset as the study mentioned in [16], which was collected from key tables such as patient demographics, diagnoses, nursing assessments, and vital periodic records. This reference dataset consisted of 138 features related to patient information, baseline measurements, labels, and temporal vital signs. There are features related to patient data, baseline physical measurements, diagnosis, label, and temporal vital signs. Patient data includes parameters like gender, age, ethnicity, weight and height. Baseline physical measurements include Glasgow coma scale (GCS), systolic blood pressure, diastolic blood pressure, mean blood pressure, pulse pressure, heart rate, respiration, and SpO2 oxygen saturation. Diagnosis includes diagnosisoffset and diagnosispriority. Label includes ICD9 codes and categories. Temporal vital sign data includes feature-lagged physical measurements.

To clean up the dataset, we removed 12 features with excessive missing values, reducing the feature count from 138 to 126. Further preparing the dataset for analysis and preventing data leakage, we excluded an additional six label-related features (e.g., ICD9, categories 1-4, and binary label) and six features used solely for preprocessing (e.g., patientunitstayid, observationoffset, activeupondischarge, diagnosisoffset, diagnosispriority, hospitaladmitoffset). Labels were generated from clinician-evaluated ICD9 codes corresponding to specific diagnoses, and the records were categorized into two groups: *sepsis* and *other*. It was notably imbalanced, with 24.4% of the samples being sepsis-positive [16]. The final dataset used to compare PDD's error detection comprised of 10,743 records, 113 features, and one label feature. Notably, while the full 114-feature dataset was compared before and after error detection using supervised learning models in section 3.4, only a 28-feature subset was used by PDD to interpret the dataset and compare unsupervised learning methods in section 3.1 and 3.2. Detailed processing steps are included in the $AppendixA$.

2.2. Methodology

In this section, we presented the proposed algorithm applied to the dataset descriptive in section 2.1. The algorithm completes three main tasks: 1) Pattern discovery via PDD for interpretability, as discussed in the [11], 2) Unsupervised learning applied to the dataset; 3) Detecting errors or abnormal samples (i.e., mislabelled records, outliers, and undecided records).

2.2.1. Interpreting Dataset

Our early work with PDD focused on interpretable pattern discovery. In this section, we presented how PDD works for interpretability. As an overwhelming number of features (attributes) can complicate interpretability, we removed redundant features and retained 27 features describing patient demographics and their physical assessments. This includes 15 features related to physical measurements and patient information (i.e., GCS, systolic blood pressure, diastolic blood pressure, mean blood pressure, pulse pressure, heart rate, respiration rate, SpO2, age, gender, ethnicity, discharge status, admission weight, discharge weight, and height); another two observation features for each of the six physical measurements, totaling 12 features; and one label feature. Consequently, the dimension of the dataset is 10,743 by 28.

Table 1. Clinician Feature Bins.

Features	Low Range	Normal Range	High Range
GCS	3-8 (Severe)	9-12 (Moderate)	13-15 (Mild)
Systolic BP[1]	<90 mm Hg	90 - 120 mm Hg	>120 mm Hg
Diastolic BP[1]	<60 mm Hg	60 - 80 mm Hg	>80 mm Hg
Mean BP[1]	<70 mm	70-93 mm Hg	>93 mm Hg
Pulse Pressure	<30 mm Hg	30 - 40 mm Hg	>40 mm Hg
Heart Rate	<60 bpm	60 - 100 bpm	>100 bpm

[1] Blood Pressure

Due to the unlimited degrees of freedom inherent in numerical features, correlating these features with the target variable and interpreting the associations present significant challenges. So, the first step of the PDD process is discretizing the numerical features into event-based or discrete categories according to clinical standards as Table 1 shows. Other numerical features without clear intervals, such as age and admission weight, were discretized into intervals that ensure a uniform distribution of data points within each interval such that each bin contains the same number of records. This method indirectly enhances the informational value of the data.

Then, on the discrete dataset, using PDD [11], we construct a statistical residual matrix (SR-Matrix) to account for the statistical strength of the associations among feature values. In pattern discovery, the term "attribute" is used instead of "feature," so "attribute value" (AV) will be used subsequently. Since the meaning of the attribute values (AVs) and their class labels are implicit, the discovery of a statistically significant association of the AVs is unaffected by prior knowledge or confounding factors. To evaluate the association between each pair of AVs in the SR-Matrix, we calculated the statistical measure of adjusted standardized residual to represent the statistical weights of the association between distinct AV pairs. For instance, if AV_1 represents the value of attribute *systolic* as H, and AV_2 represents the value of attribute *diastolic* as L. Then the adjusted standard residual of the association between AV_1 and AV_2 is calculated in equation (1), which is denoted as $SR(AV_1, AV_2)$.

$$SR(AV_1, AV_2) = \frac{Occ(AV_1, AV_2) - Exp(AV_1, AV_2)}{\sqrt{Exp(AV_1, AV_2) \cdot (1 - \frac{Occ(AV_1)}{N}) \cdot (1 - \frac{Occ(AV_2)}{N})}} \tag{1}$$

where $Occ(AV_1)$ and $Occ(AV_2)$ represent the number of occurrences of each attribute value; $Occ(AV_1, AV_2)$ is the total number of co-occurrences of the two attribute values; and $Exp(AV_1, AV_2)$ refers to the expected frequency of co-occurrences of the two attribute values; N is the total number of entities.

Subsequently, PDD applied a linear transformation, Principal Component Analysis (PCA), to decompose the SR-Matrix into Principal Components (PCs). Each PC is functionally independent, capturing unique associations distinct from those identified by other PCs. PDD then reprojected each PC back onto an SR-Matrix to generate a Reprojected SR-Matrix (RSR-Matrix) for each distinct PC. If the maximum residual between a pair of AVs within an RSR-Matrix exceeds a statistical threshold, such as 1.96, corresponding to a 95% confidence interval, the association captured is considered statistically significant. The associations discovered within each RSR-Matrix (or PC) remain functionally independent from those in other RSR-Matrices (or PCs).

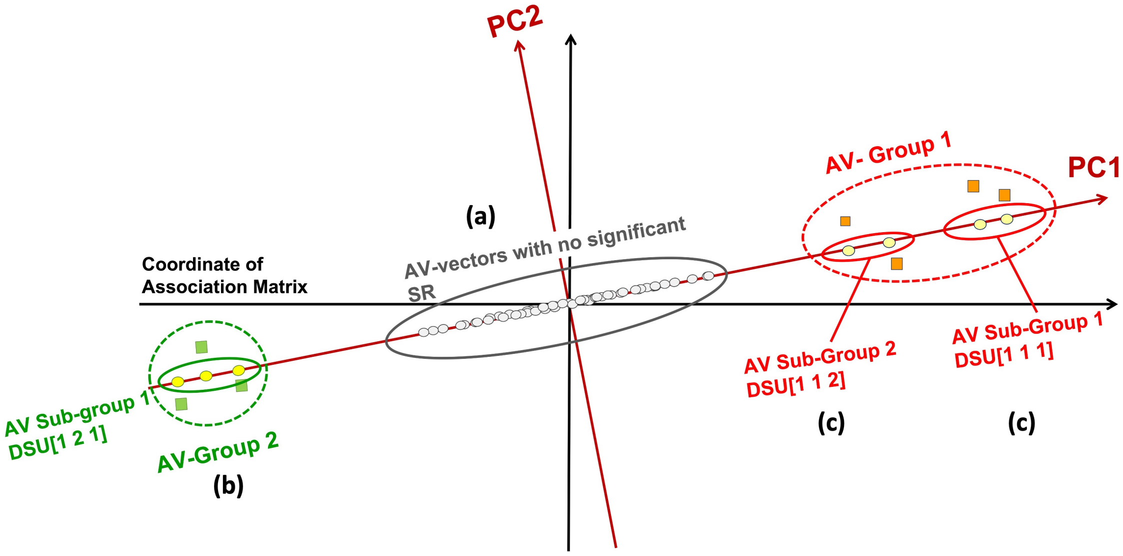
PC2
PC1
(a)
AV-vectors with no significant SR
Coordinate of Association Matrix
AV- Group 1
AV Sub-Group 2 DSU[1 1 2]
AV Sub-Group 1 DSU[1 1 1]
(c)
(c)
AV Sub-group 1 DSU[1 2 1]
AV-Group 2
(b)

Figure 1. Principal Components ($PC1$, $PC2$) with AV Groups and Subgroups discovered by PDD. (**a**) On $PC1$, AVs with no significant statistical association with other AVs (SR less than the statistical significance threshold) are projected near the origin (marked as (a)). (**b**) AV Groups with statistically significant associations are projected further from the origin, indicating strong associations with other AVs (marked as (b)). (**c**) Subgroups, denoted by Disentangled Statistical Units (DSUs), within significant AV groups (marked as (c)).

Figure 1 illustrates the concept of disengagement of AV association. After decomposing the SR-Matrix, PCs and their corresponding RSR-Matrices are obtained. Only RSR-Matrices containing SR values exceed the statistical significance threshold, and their corresponding PCs are retained. For each of those retaining PCs, as shown in Figure 1, three groups of projected AVs can be identified along its axis, each showing different degrees of statistical associations. Those close to the origin are not statistically significant and thus do not associate with distinct groups or classes (marked as (a) in Figure 1); those at one end of the projections (marked as (b)); and those at the opposite end. The AV groups or subgroups in (b), if their AVs within are statistically connected but disconnected from other

doi:10.20944/preprints202407.0425.v1

groups, may associate with distinct sources or classes (marked as (c)). As a result, two AV groups at opposite extremes were discovered. That is to say, each AV within such a group is statistically linked to at least one other AV within, and none of them is statistically connected to AVs in other groups.

Furthermore, to achieve a more detailed separation of groups, several subgroups are separated in each AV group based on their appearance in entity groups. This is done using a similarity measure defined by the overlapping of entities each AV can cover. We denote such an AV subgroup by a three-digit code $[\#PC, \#Group, \#SubGroup]$ and refer to it as a Disentangled Space Unit (DSU). We hypothesize that these DSUs originate from distinct functional sources.

Therefore, in each subgroup denoted by DSU, a set of AVs is included, which are referred to as pattern candidates. We then developed a pattern discovery algorithm to grow high-order patterns, called comprehensive patterns, from the pattern candidates. In the end, a set of high-order comprehensive patterns is generated within each DSU, and they are all associated with the same distinct source.

The interpretable output of the PDD is organized in a PDD Knowledge Base. This framework is divided into three parts: the Knowledge Space, the Pattern Space, and the Data Space. Firstly, the Knowledge Space lists the disentangled AV subgroups referred to as a Disentangled Space Unit (DSU) (denoted by a three-digit code, $[\#PC, \#Group, \#SubGroup]$ shown in the three columns of the knowledge space to indicate different levels of grouping) linking to the patterns discovered by PDD on the records. Secondly, the Pattern Space displays the discovered patterns, detailing their associations and their targets (the specified class or groups). Thirdly, Data Space shows the record IDs of each patient, linking to the knowledge source (DSU) and the associated patterns. Thus, this Knowledge Base effectively links knowledge, patterns, and data together. If an entity (i.e., a record) is labelled as a class, we can trace the "what" (i.e., the patterns it possesses), the "why" (the specific functional group it belongs to), and the "how" (by linking the patterns to the entity clusters containing the pattern(s)).

The novelty and uniqueness of PDD lie in its ability to discover the most fundamental, explainable, and displayable associations at the AV level from entities (i.e., records) associated with presumed distinct primary sources. This is based on robust statistics, unbiased by class labels, confounding factors, and imbalanced group sizes, yet its results are trackable and verifiable by other scientific methods.

2.2.2. Clustering Patient Records

Without specifying the number of clusters to direct the unsupervised process, PDD can cluster records based on the disentangled pattern groups and subgroups.

As described in section 2.2.1, the output of PDD is organized into a Knowledge Base, where each pattern subgroup is represented by a $DSU[\#PC, \#Group, \#SubGroup]$. As defined in section 2.2.1, the set of AVs displayed in each DSU is a summarized pattern, representing the union of all the comprehensive patterns on entities discovered from that subgroup. We denote the number of comprehensive patterns discovered from the summarized pattern in DSU as $\#CP - DSU$. For example, in $DSU[1,1,1]$, if 10 comprehensive patterns are found, then $\#CP[1,1,1] = 10$. Each record may possess none, one, or multiple comprehensive patterns for each DSU. We denote the number of comprehensive patterns possessed by a record in a specific DSU as $\#ID - DSU$. For example, $\#1[1,1,1] = 5$ and $\#1[2,1,1] = 6$ represent the record with $ID = 1$ possess 5 comprehensive patterns in $DSU[1,1,1]$ and 6 comprehensive patterns in $DSU[2,1,1]$.

Each DSU can represent a specific function or characteristic in the data, potentially associated with a particular class. For example, in this study, $DSU[1,1,1]$ is associated with *sepsis*, while $DSU[1,2,1]$ is associated with *other*. The fact that $DSU[1,1,1]$ and $DSU[1,2,1]$ appear as two opposite groups in $PC1$ (Figure 1) indicates that their AV associations have significant differences as captured by $PC1$. Some DSUs might reveal rare patterns not associated with any class while the class label is not in the association.

Based on the definitions described above, we cluster the records by assigning each record to the class that matches the most comprehensive patterns compared to any other class. To provide a more detailed explanation of the clustering process, consider the following example. The DSU outputted by PDD are $DSU[1,1,1]$, $DSU[1,2,1]$, $DSU[2,1,1]$, and $DSU[2,2,1]$, which are associated with *sepsis*, *other*, *sepsis*, and *other*, respectively. The total number of comprehensive patterns in these DSUs are $\#CP[1,1,1] = 100$, $\#CP[1,2,1] = 100$, $\#CP[2,1,1] = 200$, and $\#CP[2,2,1] = 200$ respectively. Consider a record $(ID = n)$ with comprehensive patterns possessed by this record are $\#n[1,1,1] = 50$, $\#n[1,2,1] = 60$, $\#n[2,1,1] = 0$, and $\#n[2,2,1] = 150$.

Due to the variation in the number of comprehensive patterns across DSUs, we use a percentage rather than an absolute value to measure the association of the record with pattern groups. Hence, to determine how the record $(ID = n)$ is associated with the *sepsis* patterns, we calculate the average percentage of the number of comprehensive patterns associated with a specific class possessed by the record, denoted as $\#ID - Class$. Due to $\#n[2,1,1] = 0$ indicates that the record is not covered by the DSU[2,1,1], it is excluded from the calculation to avoid the significant impact of a zero value on the final percentage. Hence, the association of the record $(ID = n)$ with the *sepsis* patterns is calculated as $\#n - sepsis = 50/100 = 0.5$. Similarly, $\#n - others = mean(60/100, 150/200) = 0.675$. Since $\#n - others$ is greater than $\#n - sepsis$, the record is assigned as *other*. To evaluate the accuracy of this assignment for all records, we compare the assigned class label with the original implicit class label.

2.2.3. Detecting Abnormal Records

The evaluation of the classification or prediction involves comparing the predicted labels with the original class labels. However, this comparison is unreliable if mislabels exist in the original data. To address this issue, we proposed an error detection method to identify abnormal records using the patterns discovered by PDD. In our early work on PDD, we integrated both the supervised and unsupervised methods for error detection and class association. In this paper, we simplify the process by using only a novel unsupervised method on a dataset with implicit class labels as the ground truth, making the error detection process more succinct.

To determine whether a record is abnormal, the proposed algorithm compares the class assigned by PDD with its original labels, evaluating the consistency of discovered patterns with their respective explicit or implicit class labels. We define three statuses to an abnormal record: **Mislabelled**, **Outlier**, and **Undecided**, which are detailed below.

- **Mislabelled**: If a record is categorized into one class but matches more patterns from a different class according to the PDD output, it suggests the record may be **mislabelled**. For example, consider the same record with $ID = n$ described in section 2.2.2 with the same setting of the pattern groups where $\#n - sepsis = 0.5$ and $\#n - others = 0.675$. If the record is originally labelled as *sepsis* in the dataset, but the relative difference $(|\#n - others - \#n - sepsis||\#n - others + \#n - sepsis|)$ is greater than 0.1, this suggests that the record $(ID = n)$ is more associated with *other* than with *sepsis*. The relative difference is used instead of absolute difference because it provides a scale-independent comparison of the number of patterns associated with one class to another. A value greater than 0.1 indicates that the number of patterns associated with one class is statistically significantly greater than the number associated with another class. Hence, the record $(ID = n)$ may be **mislabelled**.
- **Outlier**: If a record possesses no patterns or very few patterns, it may indicate the record is an **outlier**. For example, a record with $ID = m$ uses the previously described pattern group settings. The comprehensive patterns possessed by this record are: $\#m[1,1,1] = 1$, $\#m[1,2,1] = 0$, $\#m[2,1,1] = 0$, and $\#m[2,2,1] = 1$. Calculating the percentages, $\#m - sepsis$ is $1/100 = 0.01$ and $\#m - others$ is $1/200 = 0.005$. Both percentages are less than or equal to 0.01, suggesting that record m possesses fewer than 1% of the patterns associated with either class, which may indicate it is an **outlier**.

- **Undecided**: If the number of possessed patterns for a record is similar across different classes, the record should be classified as **undecided**. For example, a record with $ID = k$ uses the previously described pattern group settings. The comprehensive patterns possessed by this record are: $\#k[1,1,1] = 50$, $\#k[1,2,1] = 60$, $\#k[2,1,1] = 110$, and $\#k[2,2,1] = 100$. Calculating the percentages, $\#k - sepsis$ is the mean of 50/100 and 110/200, which is 0.55; and $\#k - others$ is the mean of 60/100 and 100/200, which is 0.55. Since the difference between the two percentages is zero or less than 0.001, record k may be associated with both classes, suggesting it is **undecided**

To avoid adding new incorrect information, mislabelled, undecided, and outliers are removed from the dataset. Hence, to validate the effectiveness of abnormal records detected by PDD, we compared classification results from the original dataset to those from a dataset without abnormal records when various classifiers were applied.

3. Results

The experimental results are presented in this section. First, section 3.1 demonstrates the interpretable output derived from PDD. Next, section 3.2 compares PDD's clustering accuracy with the K-means algorithm which serves as our baseline. Then, section 3.3 presents our error detection results, showing interpretable outcomes with discovered patterns after mislabeling detection. Finally, section 3.4 demonstrates the efficacy of error detection by comparing the performance of supervised learning algorithms both before and after the application of error detection.

3.1. Interpretable Results

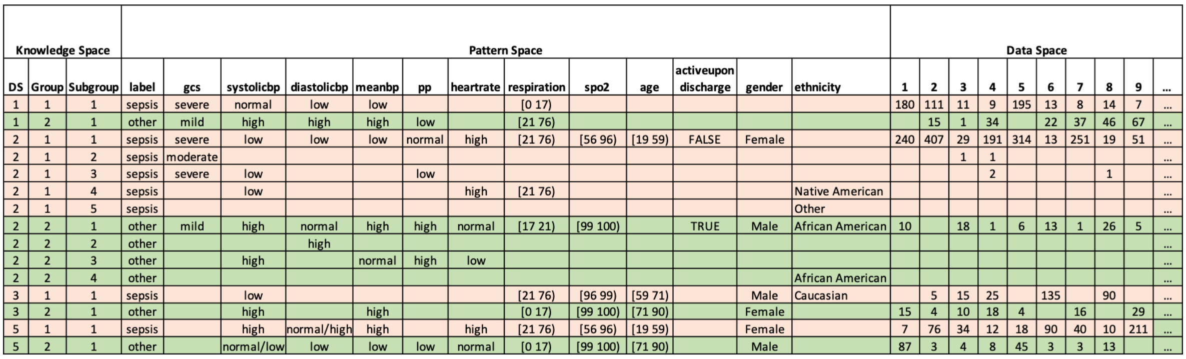

Knowledge Space			Pattern Space													Data Space									
DS	Group	Subgroup	label	gcs	systolicbp	diastolicbp	meanbp	pp	heartrate	respiration	spo2	age	activeupon discharge	gender	ethnicity	1	2	3	4	5	6	7	8	9	...
1	1	1	sepsis	severe	normal	low	low			[0 17)						180	111	11	9	195	13	8	14	7	...
1	2	1	other	mild	high	high	high	low		[21 76)							15	1	34		22	37	46	67	...
2	1	1	sepsis	severe	low	low	low	normal	high	[21 76)	[56 96)	[19 59)	FALSE	Female		240	407	29	191	314	13	251	19	51	...
2	1	2	sepsis	moderate														1	1						...
2	1	3	sepsis	severe	low			low											2				1		...
2	1	4	sepsis		low				high	[21 76)					Native American										...
2	1	5	sepsis												Other										...
2	2	1	other	mild	high	normal	high	high	normal	[17 21)	[99 100)		TRUE	Male	African American	10		18	1	6	13	1	26	5	...
2	2	2	other			high																			...
2	2	3	other		high		normal	high	low																...
2	2	4	other												African American										...
3	1	1	sepsis		low					[21 76)	[96 99)	[59 71)		Male	Caucasian		5	15	25		135		90		...
3	2	1	other		high		high			[0 17)	[99 100)	[71 90)		Female		15	4	10	18	4		16		29	...
5	1	1	sepsis		high	normal/high	high		high	[21 76)	[56 96)	[19 59)		Female		7	76	34	12	18	90	40	10	211	...
5	2	1	other		normal/low	low	low	low	normal	[0 17)	[99 100)	[71 90)		Male		87	3	4	8	45	3	3	13		...

Figure 2. Knowledge Base outputted by PDD.

In this section we present interpretable results, via the PDD knowledge base, containing all summarized patterns from different DSUs in Figure 2. The knowledge base contains three parts: the knowledge space, the pattern space, and the data space. First, the Knowledge Space uses the triple code of the DSU to indicate the primary source that gives rise to the disentangled patterns from the AV Subgroup. In this specific study, as shown in Figure 2, the first row displays the group discovered as the first disentangled space denoted by the code $[1,1,1]$, indicating in reverse order the first Sub-Pattern group (SubGroup) of the first Pattern Group (Group) discovered in the first Principal Component (PC). Here, we identify two groups corresponding to two types of diseases: *sepsis* and *other*. The results show all DSUs discovered by PDD representing all the disentangled spaces with statistically significant patterns obtained from the first three PCs.

Second, the Pattern Space reveals the specific AV association patterns and their targets (the specified class or groups, if given) obtained from the DSU. We find that the disease *sepsis* exhibits different patterns than *other*. For example, the *sepsis* class was associated with lower blood pressure, higher heart rate, higher respiration, and moderate or severe GCS. Inversely, the *other* class was associated with higher blood pressure, normal heart rate, lower respiration, and mild GCS. Since the patterns outputted by PDD are disentangled, they clearly distinguish between the different classes of *sepsis* and *other*.

The patterns related to sepsis demonstrate clinical relevance as hypotension, tachycardia, elevated respiratory rate, and altered mental status are all considered key criteria defined in the Third International Consensus for Sepsis and Septic Shock (Sepsis-3)[17]. Singer et al. [17] discussed how septic shock is associated with underlying circulatory, cellular, and metabolic abnormalities that substantially increase mortality. These characteristic abnormalities helped to improve understanding of sepsis pathobiology and informed treatment such as a vasopressor requirement to constrict blood vessels and maintain a minimum mean arterial pressure in the absence of hypovolemia or adequate fluid resuscitation. This shows evidence of a positive correlation between low blood pressure and the severity of sepsis among patients with septic shock, which is consistent with patterns discovered by PDD. In addition to this, sepsis is impacted by various biomarkers and physiological parameters, such as C-reactive protein, white blood cell count, and central venous pressure [18][19]. Thus, with a more detailed dataset, PDD can further examine associations between sepsis and these factors.

Thirdly, the Data Space displays the records with their IDs from the original dataset and the discovered patterns each record possesses. As shown in Figure 2, the number in the column of each ID on the row linking to the pattern(s) and the DSU(s) represents the number of the comprehensive patterns in a DSU that the record possesses. For example, 180 indicates there are 180 comprehensive patterns in the $DSU[1,1,1]$ covered by record 1. Due to space limitations, only the first nine records $(ID = 1 \text{ to } 9)$ are displayed.

In the original data, records labelled *sepsis* are listed before those labelled *other*, so the first nine records belong to the *sepsis* class. It is also evident in the Data Space that the records possess more patterns associated with *sepsis* than with *other*.

3.2. Comparison of Unsupervised Learning

In addition, we compared the PDD's clustering results with the classical clustering algorithm K-mean as the baseline. For a clear comparison, both the same subset $(10,743 \times 28)$ and the full dataset $(10,743 \times 114)$ were used to evaluate K-means performance. To run K-means, we used the *sklearn.clusters* package in Python 3.0 [20] with all default parameter settings and assigned the number of clusters as two, as the original data only contains the two classes of *sepsis* and *other*.

To evaluate an imbalanced dataset, balanced accuracy is more reliable than regular accuracy. Using regular accuracy, a model might frequently predict the majority class and still achieve a high accuracy rate, despite failing to accurately predict the minority class [21]. Balanced accuracy, however, considers the true positive rate of each class, offering a more honest evaluation of model performance, which is essential when one class significantly outnumbers another. Therefore, we utilize both balanced accuracy and accuracy for evaluating classification or clustering performance, in addition to precision, recall, and a weighted F1-score for comparison.

Table 2. Comparison between PDD and K-means for unsupervised learning.

Unsupervised Learning	Precision	Recall	Accuracy	Balanced Accuracy	Weighted F1-Score
PDD (28-features data)	0.83	0.90	0.87	**0.89**	0.88
K-means (28-features data)	0.43	0.42	0.52	**0.42**	0.54
K-means (114-features data)	0.59	0.51	0.75	**0.51**	0.67

Based on the unsupervised clustering results in Table 2, PDD significantly outperformed K-Means on both the 28-feature subset and 114-feature dataset. On the 28-feature subset, the balanced accuracy of 0.89 achieved with PDD was significantly higher than the 0.42 achieved with K-means. On the 114-feature dataset, K-means exhibited improved performance, demonstrating the benefit of including more features. However, even when comparing PDD's performance on the reduced feature subset to K-means performance on the full feature dataset, PDD still outperformed K-means by 38%.

The two clustering methods were also compared in terms of their effectiveness in handling dataset imbalance, given that only 24.4% of samples were sepsis-positive. As shown in Table 2, PDD's balanced accuracy on the 28-feature subset exceeds regular accuracy indicating a more effective prediction of the minority class *sepsis*. In contrast, K-means' regular accuracy exceeds balanced accuracy on both the 28 and 114-feature datasets indicating a more effective prediction of the majority class *other*. Moroever, the difference between the accuracy and balanced accuracy of PDD results is a minimal 2% in comparison to K-means' results with differences of 10% and 24%. This indicates that PDD is better suited for handling imbalanced data and is a valuable tool for datasets where accurate prediction of the minority class is crucial. Also, that PDD has learned meaningful patterns in the minority class despite its scarcity in the dataset while K-means struggles to accurately capture these characteristics and is therefore challenged by the imbalanced distribution. In this case, PDD not only predicts more accurate clustering results for the minority class but also provides patterns that reveal the characteristics of the cluster. PDD can display all the statistically significant patterns with their source (DSU) possessed by each cluster. It also corrects mislabels based on its error detection capability and the records' implicit class labels.

3.3. Error Detection Results

This section presents the error detection results using the PDD knowledge base. As mentioned in 2.2.3 and 3.1, we used the comprehensive pattern count from the PDD data space to detect abnormal records in the original dataset. For example, $ID = 5510$ has $\#5510[1,1,1] = 30$, $\#5510[2,1,1] = 13$, $\#5510[3,1,1] = 2$, $\#5510[5,1,1] = 6$, and all DSU is associated with *sepsis*. Thus, $\#5510 - sepsis = mean(30/1357, 13/2617, 2/453, 6/940) \approx 0.0095$. Similarly, $\#5510[1,2,1] = 2$, $\#5510[2,2,1] = 51$, $\#5510[3,2,1] = 3$, $\#5510[5,2,1] = 8$, thus $\#5510 - other = mean(2/696, 51/2514, 3/561, 8/1712) \approx 0.0083$. Both $\#5510 - sepsis$ and $\#5510 - other$ are less than the threshold 0.01 specified in 2.2.3, $ID = 5510$ is categorized as an outlier.

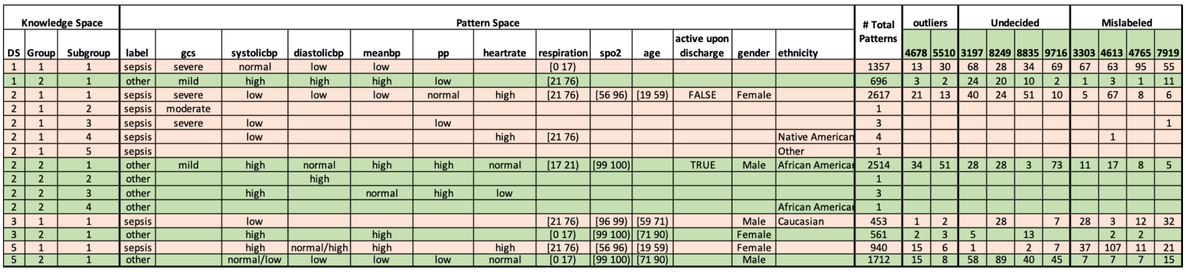

Knowledge Space			Pattern Space													# Total Patterns	outliers		Undecided				Mislabeled			
DS	Group	Subgroup	label	gcs	systolicbp	diastolicbp	meanbp	pp	heartrate	respiration	spo2	age	active upon discharge	gender	ethnicity		4678	5510	3197	8249	8835	9716	3303	4613	4765	7919
1	1	1	sepsis	severe	normal	low	low			[0 17)						1357	13	30	68	28	34	69	67	63	95	55
1	2	1	other	mild	high	high	high	low		[21 76)						696	3	2	24	20	10	2	1	3	1	11
2	1	1	sepsis	severe	low	low	low	normal	high	[21 76)	[56 96)	[19 59)	FALSE	Female		2617	21	13	40	24	51	10	5	67	8	6
2	1	2	sepsis	moderate												1										
2	1	3	sepsis	severe	low			low								3										1
2	1	4	sepsis		low				high	[21 76)					Native American	4								1		
2	1	5	sepsis												Other	1										
2	2	1	other	mild	high	normal	high	high	normal	[17 21)	[99 100)		TRUE	Male	African American	2514	34	51	28	28	3	73	11	17	8	5
2	2	2	other			high										1										
2	2	3	other		high		normal	high	low							3										
2	2	4	other												African American	1										
3	1	1	sepsis		low					[21 76)	[96 99)	[59 71)		Male	Caucasian	453	1	2		28		7	28	3	12	32
3	2	1	other		high		high			[0 17)	[99 100)	[71 90)		Female		561	2	3	5		13			2	2	
5	1	1	sepsis		high	normal/high	high		high	[21 76)	[56 96)	[19 59)		Female		940	15	6	1		2	7	37	107	11	21
5	2	1	other		normal/low	low	low	low	normal	[0 17)	[99 100)	[71 90)		Male		1712	15	8	58	89	40	45	7	7	7	15

(a)

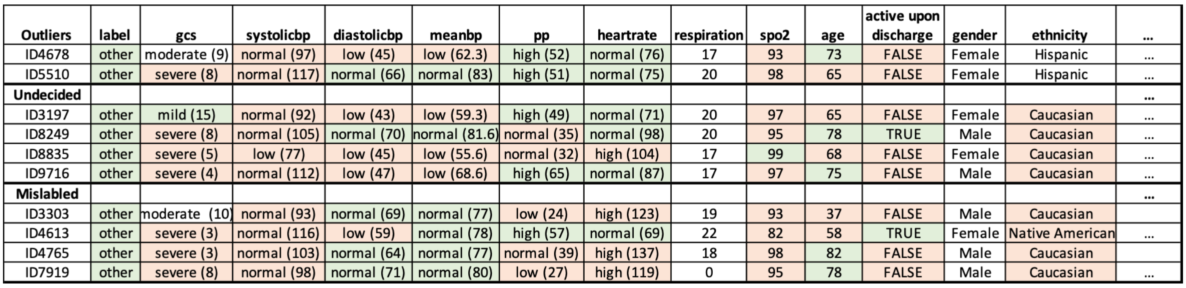

Outliers	label	gcs	systolicbp	diastolicbp	meanbp	pp	heartrate	respiration	spo2	age	active upon discharge	gender	ethnicity	...
ID4678	other	moderate (9)	normal (97)	low (45)	low (62.3)	high (52)	normal (76)	17	93	73	FALSE	Female	Hispanic	...
ID5510	other	severe (8)	normal (117)	normal (66)	normal (83)	high (51)	normal (75)	20	98	65	FALSE	Female	Hispanic	...
Undecided														...
ID3197	other	mild (15)	normal (92)	low (43)	low (59.3)	high (49)	normal (71)	20	97	65	FALSE	Female	Caucasian	...
ID8249	other	severe (8)	normal (105)	normal (70)	normal (81.6)	normal (35)	normal (98)	20	95	78	TRUE	Male	Caucasian	...
ID8835	other	severe (5)	low (77)	low (45)	low (55.6)	normal (32)	high (104)	17	99	68	FALSE	Female	Caucasian	...
ID9716	other	severe (4)	normal (112)	low (47)	low (68.6)	high (65)	normal (87)	17	97	75	FALSE	Male	Caucasian	...
Mislabled														...
ID3303	other	moderate (10)	normal (93)	normal (69)	normal (77)	low (24)	high (123)	19	93	37	FALSE	Male	Caucasian	...
ID4613	other	severe (3)	normal (116)	low (59)	normal (78)	high (57)	normal (69)	22	82	58	TRUE	Female	Native American	...
ID4765	other	severe (3)	normal (103)	normal (64)	normal (77)	normal (39)	high (137)	18	98	82	FALSE	Male	Caucasian	
ID7919	other	severe (8)	normal (98)	normal (71)	normal (80)	low (27)	high (119)	0	95	78	FALSE	Male	Caucasian	...

(b)

Figure 3. Error Detection results by PDD. (**a**) Knowledge Base of partial abnormal records. (**b**) Partial abnormal records of the original dataset.

In total, PDD identified 996 mislabelled records, 2 outliers, and 159 undecided records. To avoid adding new incorrect information, we finally removed the 1157 records, and 9586 records were retained. For simplicity, only a partial result is shown in Figure 3

For better visualization, in Figure 3a, all the DSUs with $label = sepsis$ are highlighted in red, and all the DSUs with $label = other$ are highlighted in green. An important observation after such highlighting is that attributes are consistent within its class. For example, for all DSUs with $label = sepsis$, their blood pressure features (i.e., $systolicbp$, $diastolicbp$, $meanbp$) are mostly low. And for all DSUs with $label = other$, their blood pressure attributes are mostly high. Due to this consistency, we assigned the same highlighting scheme to specific AV in Figure 3b. For example, when $systolicbp = low$, we highlighted the AV in red, implying its positive correlation with sepsis through PDD's Pattern Space. With such a highlighting scheme, one can easily observe the pattern entanglement among the original dataset and how well PDD can disentangle the source attributes with a statistically supported, interpretable knowledge base.

3.4. Error Detection Applied to Supervised Learning Models

To demonstrate the effectiveness of the error detection methods, we compared the classification results of various classifiers on the dataset before and after removing errors. The classifiers tested include Random Forest, SVM, Neural Networks, Logistic Regression, LightGBM, and XGBoost. 80% of the data are used for training and 20% for testing. To evaluate the results, the same metrics (i.e., Precision, Recall, Accuracy, Balanced Accuracy, and Weighted F1-Score) are used for comparison.

Table 3. Results of the Accuracy of Existing ML Models Before and After Error Detection Using PDD.

Classifiers (Before/After Error Detection)	**Precision**	**Recall**	**Accuracy**	**Balanced Accuracy**	**Weighted F1-Score**
Random Forest	0.85/0.87	0.73/0.76	0.86/0.86	**0.73/0.76**	0.84/0.85
SVM	0.71/0.71	0.53/0.54	0.77/0.75	**0.53/0.54**	0.7/0.68
NN	0.71/0.74	0.71/0.80	0.79/0.77	**0.71/0.80**	0.79/0.78
Logistic Regression	0.84/0.83	0.79/0.80	0.87/0.86	**0.79/0.80**	0.87/0.86
LightGBM	0.9/0.93	0.89/0.93	0.92/0.95	**0.89/0.93**	0.92/0.95
XGBoost	0.89/0.94	0.88/0.93	0.92/0.95	**0.88/0.93**	0.92/0.95

Table 3 shows the comparison results of existing ML models before and after error detection. This error detection process by PDD resulted in an accuracy improvement of approximately 1% - 9% and 4% on average. The error detection results show how PDD can remove those abnormal records (outliers/undecided/mislabelled) to improve the accuracy of class association for building a classifier based on a cleaner training set since the balanced accuracy is increased for all classifiers.

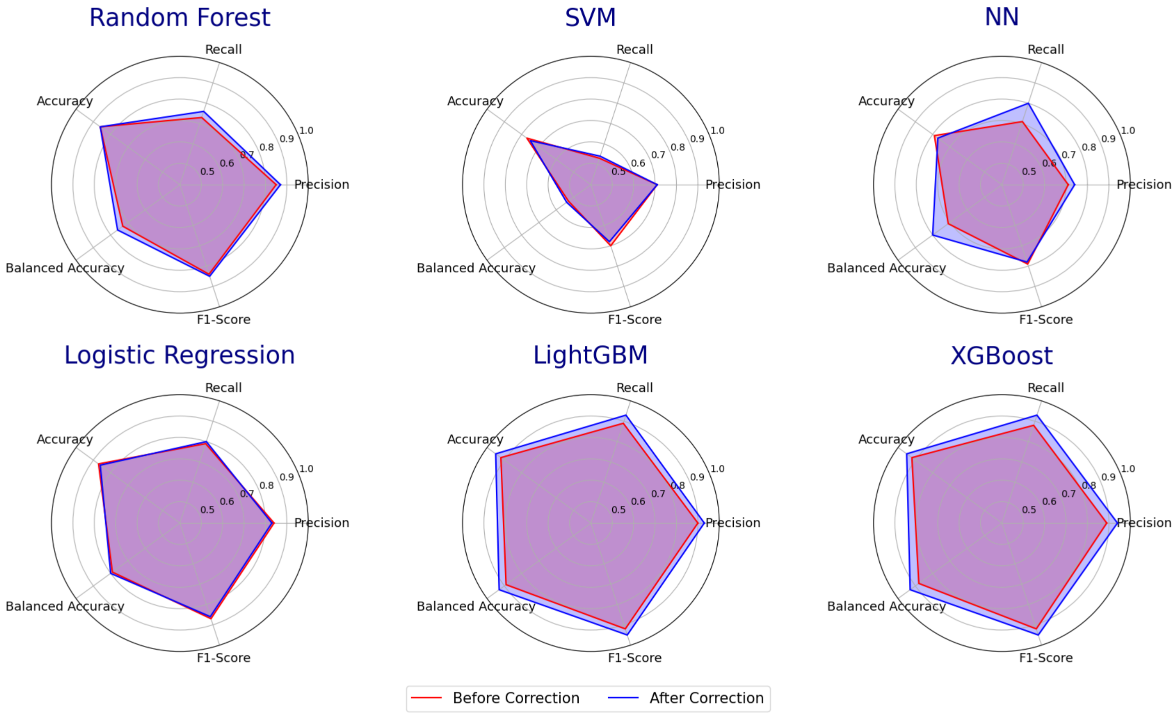

Figure 4. Comparison of the Accuracy of Classifiers Before and After Error Detection.

In Table 3, it is also interesting to note how different classifiers handle overfitting and bias in imbalanced data with varying capabilities. First, for all classifiers, the regular accuracies are greater than the balanced accuracies, indicating that the predictions are more effective for the majority class, particularly for the first four traditional classifiers (RF, SVM, NN, and LR). However, for models with class balancing capability (LightGBM and XGBoost), the differences between regular accuracy and balanced accuracy are small. Second, the higher accuracy before error detection indicates that models are performing better on the majority class, which can be a sign of overfitting to the majority class. So the accuracy slightly decreases after removing abnormal cases due to reducing the overfitting for the majority class. Lastly, after error detection, the balanced accuracies increase. This indicates that outliers and undecided cases were biasedly absorbed into the majority classes before error detection, but after error detection, the classifiers show better prediction results for the minority class, leading to better results for the balanced prediction.

Additionally, to effectively highlight comparison results, Figure 4 displays radar charts that visualize each classifier's overall performance profile. These charts distinctly show that the blue areas, representing improved metrics, are larger than the red areas for all models, with particularly obvious differences in LightGBM and XGBoost.

4. Discussion

In this section, we discuss the results of interpretability and error detection using PDD from the perspective of previous studies.

4.1. Interpretability

Decision Trees are widely regarded as interpretable models, and similarly, Random Forests (RF) can also provide interpretable insights despite being less straightforward due to their ensemble nature. Various methods have been developed to extract feature importance or feature contributions to enhance its interpretability [22]. In this section, we compare the interpretability between RF and PDD.

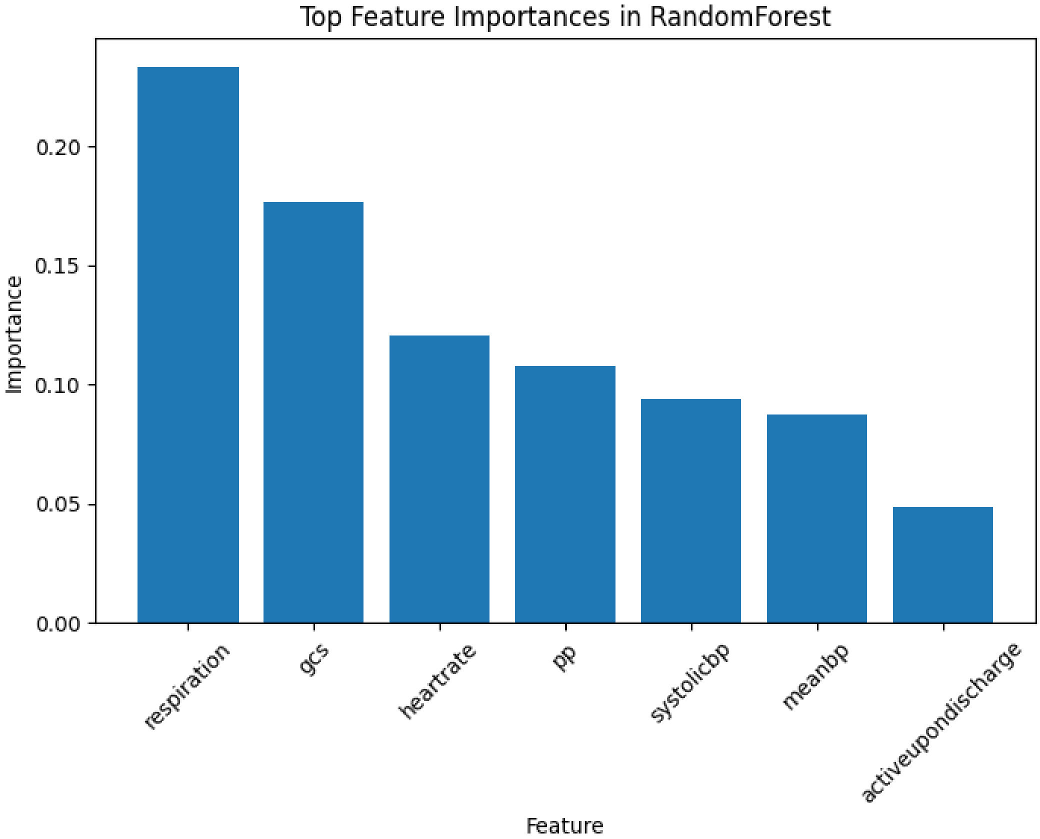

Figure 5. Top feature importances associated with class labels outputted by the Random Forest Model.

First, according to the RF model illustrated in Figure 5, RF assesses the importance of features associated with class labels. Similarly, as shown in Figure 2, PDD discovers patterns that reveal the associations between feature values rather than just feature associations.

Second, the importance analysis provided by RF shows the association between one feature and the target, while PDD goes further by revealing the significance of high-order comprehensive patterns linked to the target, which provides a more direct, succinct, precise, and interpretable understanding of the problem. This capability allows PDD to provide a more in-depth and precise interpretation, which is crucial for high-stakes applications requiring transparency and explainability.

Lastly, RF can also output prediction rules similar to the high-order patterns in PDD. However, according to the supervised learning comparison results provided in section 3.4, before error detection, the accuracy of Random Forest is 86%, while the balanced accuracy is only around 73%. This indicates that, for imbalanced classes, the rules outputted by RF are easily biased towards the majority class. In contrast, as demonstrated in the study [11], PDD can discover disentangled patterns even for imbalanced data. Furthermore, PDD uses hierarchical clustering to highlight the independent functions of each pattern group, enhancing interpretability. It generates a knowledge base linking patterns, entities, and classes, which can trace the origins of the discovered patterns. This capability ensures the accuracy of error detection. This level of detail and traceability is a limitation of the RF model.

4.2. Error Detection

Real-world data may contain inconsistencies due to incorrect data collection, human errors, equipment inaccuracies, and missing values [23]. So removing errors and cleaning data is essential in developing a reliable ground truth for training and testing. In this study, the conditions of patients with sepsis may be various, leading to fluctuations that complicate establishing baseline values. The eICU-CRD dataset, collected in 2014 and 2015, predates the sepsis definition updated in 2016 [17], with the initial definition in 2001. Thus, the labels in the dataset may not reflect the latest medical insights. Furthermore, integrating data from various hospitals with different environments, procedures, equipment, and staff may introduce non-standardized variables.

PDD's error detection results in section 3.4 demonstrate removing abnormal data and creating a more reliable ground truth can improve model performance. The interpretability of PDD enables it to discover and disentangle patterns, which can be used to assign status – mislabelled, outlier, and undecided – to records. The traceability of PDD allows humans to trace patterns back to the data and clarify why a particular sample should be corrected. Furthermore, unlike other existing error detection methods that rely on model predictions, PDD is model-independent.

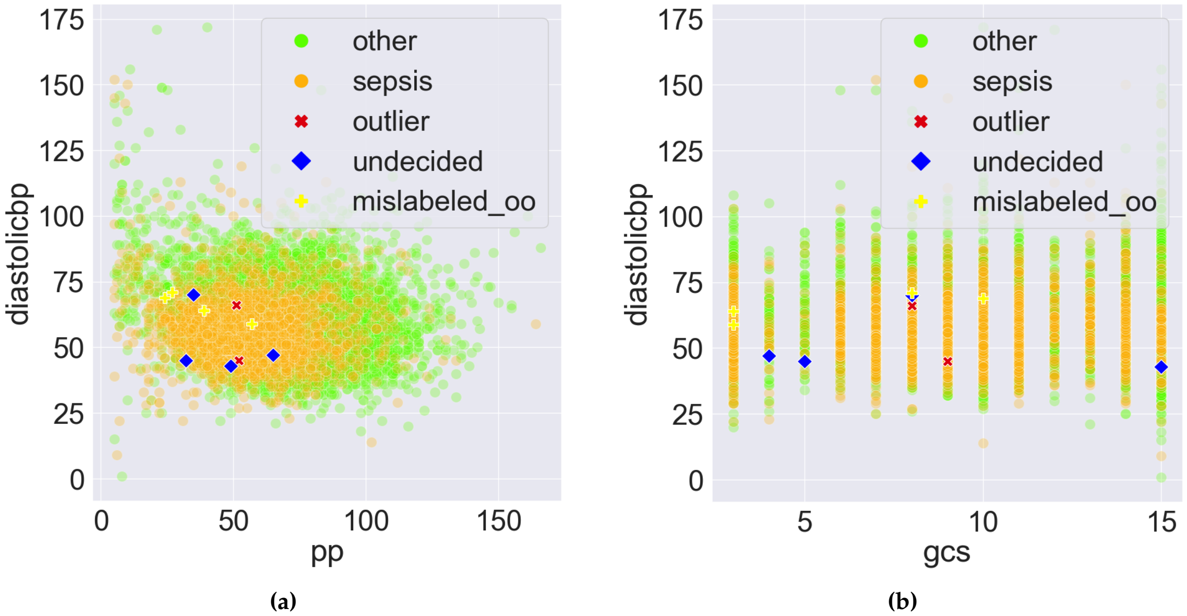

Figure 6. Sample scatter pair plots of the eICU-CRD dataset. All records are plotted. The 10 abnormal records presented in Section 3.3 are highlighted, which comprise 2 outliers, 4 undecided, and 4 mislabelled records originally labelled as *other*, denoted by *mislabelled_oo*. (**a**) *diastolicbp* vs. *pp*. (**b**) *diastolicbp* vs. *gcs*.

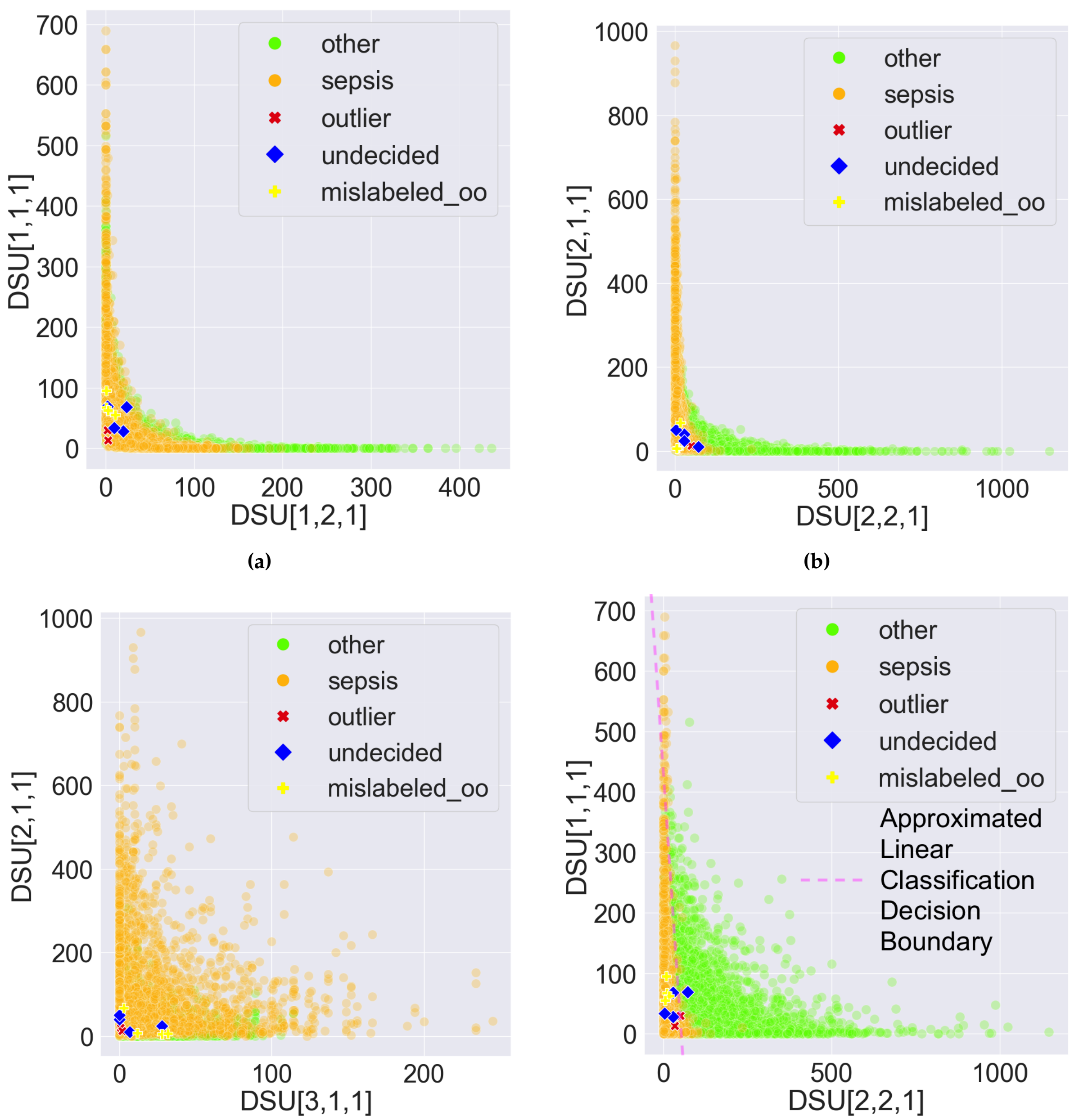

(a)

(b)

(c)

(d)

Figure 7. Sample scatter pair plots of the Data Space in the Pattern Discovery and Disentanglement (PDD)'s output. The Disentangled Space Units (DSU) in PDD are used as features, and the comprehensive pattern counts as the feature values. All records from the eICU-CRD dataset are plotted. The 10 abnormal records presented in Section 3.3 are highlighted, which comprise 2 outliers, 4 undecided, and 4 mislabelled records originally labelled as *other*, denoted by *mislabelled_oo*. (**a**) $DSU[1,1,1]$ vs. $DSU[1,2,1]$. (**b**) $DSU[2,1,1]$ vs. $DSU[2,2,1]$. (**c**) $DSU[2,1,1]$ vs. $DSU[3,1,1]$. (**d**) $DSU[1,1,1]$ vs. $DSU[2,2,1]$.

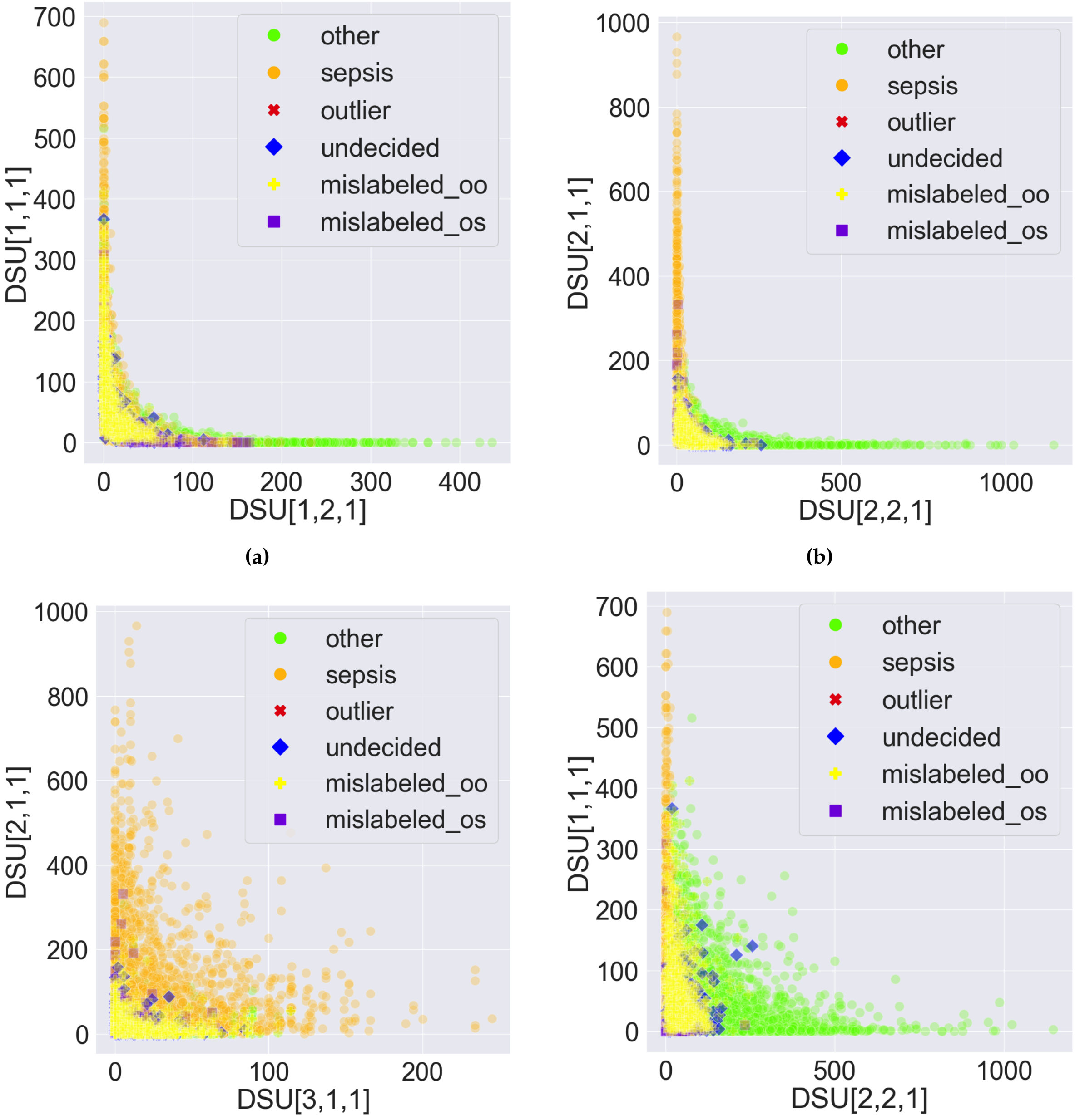

(a)

(b)

(c)

(d)

Figure 8. Sample scatter pair plots of the Data Space in the Pattern Discovery and Disentanglement (PDD)'s output. The Disentangled Space Units (DSU) in PDD are used as features, and the comprehensive pattern counts as the feature value. All records from the eICU-CRD dataset are plotted. All the 1157 abnormal records are highlighted, which comprise 2 outliers, 159 undecided and 996 mislabelled records. *mislabelled_oo* represents the 894 mislabelled records originally labelled as *other*, and *mislabelled_os* represents the 102 mislabelled records originally labelled as *sepsis*. (**a**) $DSU[1,1,1]$ vs. $DSU[1,2,1]$. (**b**) $DSU[2,1,1]$ vs. $DSU[2,2,1]$. (**c**) $DSU[2,1,1]$ vs. $DSU[3,1,1]$. (**d**) $DSU[1,1,1]$ vs. $DSU[2,2,1]$.

To better understand PDD's error detection, sample scatter pair plots between the features of the eICU-CRD dataset are shown in Figure 6. The outlier, undecided, and mislabelled records are the 10 abnormal records presented in Section 3.3. In Figure 6a and 6b, regardless of whether the x-axis values are continuous or discrete, the decision boundaries for classification are not linear. Two classes are mixed, making classification and error detection based on the original features challenging due to entanglement.

However, the two classes can be visually disentangled in PDD's Data Space as shown in Figures 7 and 8 by treating each DSU as a distinct feature and the comprehensive pattern count as the feature value. The only difference between Figures 7 and 8 is the proportion of the abnormal records that are highlighted. Figure 7 highlights the 10 abnormal records from Section 3.3. Figure 8 highlights all the 1157 abnormal records, which comprise 996 mislabelled, 2 outliers, and 159 undecided records. The DSU plot shows a more prominent classification decision boundary.

Specifically, in Figure 7a and Figure 7b, the DSUs of the x and y axes are found at the two opposite ends of the same PC, as demonstrated in Figure 1. So, if one DSU captures the AV associations solely from class *sepsis*, the other DSU should capture the AV associations solely from class *other*. By observation, Figure 7b has a more prominent classification decision boundary than Figure 7a, suggesting that PC2's clustering of the opposite groups of AV Associations is better aligned with the expected classification than PC1. The classification decision boundary can be curved as in Figure 7b, or approximated by a straight line as in Figure 7d. Both demonstrate the disentanglement capability of PDD.

All abnormal samples are highlighted in the figures. First, some of the undecided records are close to the decision boundary, as shown in Figures 7a, 7b, and 7d, since these records possess almost an equal number of patterns from both classes. It is more obvious in Figures 8b and 8d since the two classes are more disentangled. Second, most of the mislabelled records are consistently found in the *sepsis* cluster in Figures 7 and 8,. Specifically, 894 of the 996 (90%) mislabelled records were originally labelled as *other* but suggested as *sepsis*. According to the highlighted mislabeled records, this is more evident in Figures 8b and 8d since the two classes are more disentangled. Furthermore, all outlier records are situated close to the origin because they possess few patterns. Due to the unavoidable overlapping issue, this is more observable in Figure 7. Lastly, when the DSUs of both axes are associated with the same class but from different PCs, which is *sepsis* in Figures 7c and 8c, the classification decision boundary is not as clear as in *other* figures when the DSU pairs are associated with different classes as in Figures 7a, 7b, 7d and 8a, 8b, 8d.

5. Conclusions

In this study, we applied our Pattern Discovery and Disentanglement (PDD) methodology to healthcare data analysis, addressing challenges like mislabeling, class imbalance, and the need for explainable AI. The uniqueness and novelty of PDD lie in its ability to discover fundamental, explainable associations at the feature value level, unbiased by class labels, confounding factors, or imbalanced group sizes. PDD generates a comprehensive knowledge base that links patterns, entities, and sources/classes, providing deep insights and enhancing the interpretability of the results. After detecting the errors (i.e., outliers, undecided, and mislabelled), the original dataset can be cleaned. In this study, using the eICU-CRD data for sepsis risk assessment, PDD demonstrated significant improvements over traditional K-means clustering, achieving a 38% improvement on the full dataset and a 47% improvement on the reduced dataset. PDD's error detection identified 996 mislabelled records, 2 outliers, and 159 undecided cases, resulting in the removal of 1157 abnormal records. This process improved the accuracy of multiple supervised ML models by an average of 4%, with improvements ranging from 1% to 9%. The analysis highlighted PDD's ability to handle patterns challenging for traditional models, particularly lower-order patterns with limited feature correlation.

In conclusion, PDD offers a robust and practical solution for unsupervised clustering and error detection in large-size and low-quality healthcare data, enhancing both the stand-alone performance and the results of other ML models. Its application to this large, complex dataset demonstrates its practicality and effectiveness. Future work will extend PDD to other medical conditions and datasets, further validating its utility and impact in diverse healthcare applications.

Author Contributions: Conceptualization, P.Z. A.W, and S.L; methodology, P.Z., A.W, and T.W; software, P.Z., F.L., and T.W.; validation, P.Z., and A.W; formal analysis, P.Z., investigation, P.Z., T.W., and F.L.; resources, C.D and S.L.; data curation, C.D. and S.L.; writing—original draft preparation, P.Z., F.L., T.W., and A.W.; writing—review and editing, P.Z., F.L., T.W., and A.W.; visualization, P.Z., and T.W.; supervision, P.Z., and A.W.; project administration, P.Z.; funding acquisition, A.W., and S.L.. All authors have read and agreed to the published version of the manuscript.

Funding: This research was funded by NSERC I2I Phase I Grant

Data Availability Statement: Access to the eICU Collaborative Research Database can be requested at https://eicu-crd.mit.edu/

Conflicts of Interest: The authors declare no conflicts of interest.

Abbreviations

The following abbreviations are used in this manuscript:

ML	Machine Learning
EHR	electronic health records
PDD	Pattern Discovery and Disentanglement
eICU-CRD	eICU Collaborative Research Database
GCS	Glasgow coma scale
SPO2	oxygen saturation
SR	adjusted standard residual
SR-Matrix	statistical residual matrix
RSR-Matrix	Reprojected SR-Matrix
AV	attribute value
PCA	Principal Component Analysis
DSU	Disentangled Space Unit
SubGroup	Sub-Pattern group
Group	Pattern Group
PC	Principal Component
RF	Random Forests

Appendix A. Dataset Description and Preprocessing Details

These steps outline the process by which the reference dataset, with 138 features, from Parmar et al. [16] was obtained, and how this dataset was further processed to obtain the final 114 feature dataset for this paper's analysis.

Appendix A.1. Step 1: Generate Temporal Features based on Vital Signs

First, the vital periodic table contains vital sign data generated from one minute averages and archived as five minute median values at timepoints that can be identified by their observationOffset. Notably, although the dataset claims to be standardized, many of these values are missing data and not actually aligned to five-minute intervals. Every "group" contains temporal vital sign observations over a selected six-hour period. The period begins at a specific observationOffset and contains values recorded at subsequent time points. It must also contain a diagnosisOffset. The diagnosisOffset is the time since admission before a diagnosis was recorded. Patients can have multiple diagnoses during their ICU stay. The objective was to select suitable six-hour periods and align time points to five-minute intervals. To ensure diagnosisOffset was always present within the period, the search began with the first diagnosisOffset after skipping the first hour after ICU admission, which is considered an unstable period. A six-hour total period was determined by retrieving a three-hour window before the diagnosisOffset followed by a three-hour backend length. The three-hour window would be used for prediction and the three-hour backend for labeling. This process was repeated for the next available diagnosisOffset after a minimum three-hour buffer time to avoid overlap. Time points were manually added using fill-forward and fill-backward to fill in missing values and standardize them to five-minute intervals. To prioritize reliance on observed rather than manually added data, groups were filtered to select those where the actual observation offsets constitute at least half of the duration covered by manually added time points. Moreover, groups with more than 20 missing time points, out of the total 72 five-minute intervals, were filtered. For each group, the mean blood pressure must be less than systolic and diastolic blood pressure. If not, these values were replaced with NaN and then filled with the same techniques for missing values. This data was then used to generate lagged features and lagged Fourier-transformed features to identify trends and cyclical patterns. Mean, standard deviation, minimum, maximum, kurt, and skew were also calculated and added as features without look-ahead bias. The final dataset used timepoints 2 and 14 which were one hour apart.

Appendix A.2. Step 2: Process Labels

Next, labels were first created using diagnosisString based on clinician evaluation at the time. They were relabelled afterward using the calculated qSOFA score for sepsis. The diagnosis string column contains a string made up of four different categorical diagnoses split by pipe. These were separated into four new columns named Categories 1 - 4. Only patients with diagnosisPriority as primary was considered. Groups labelled as sepsis included entries where the string 'sepsis' or 'septic shock' appeared under Category 3. Groups labelled as 'other' included entries with conditions within the top 20 diseases in the dataset under Category 3. The calculated qSOFA score was used to relabel all groups. The Third International Consensus Definition for Sepsis (Sepsis-3) was updated in 2016 with an acute increase in SOFA score of 2 or more, from baseline, in a patient with suspected infection associated with a minimum twofold increased risk of death. At least two of the following clinical criteria together would constitute a new bedside clinical score termed quick sofa (qSOFA): systolic blood pressure of 100 mmHg or less, respiratory rate of 22 breaths/min or higher, and Glasgow Coma scale (GCS) less than 15 [17]. The last three hours of each group were used to calculate qSOFA . Groups were removed if the qSOFA score did not match the doctor's diagnosis for more than time.

Appendix A.3. Step 2: Filter Features

Further filtering was used to obtain the same dataset with 138 features used in Parmar et al: dropping columns with all null values, caused by lagged feature generation and inputting ethnicity with a simple input using the 'most frequent' strategy. Lastly, the final processed dataset with 10,743 records and 114 features, for this paper's analysis, was obtained by removing encoded binary values, removing label-related features to avoid leaking information (ICD9, categories 1-4, and label), and removing unnecessary features only used for preprocessing (patientunitstayid, observationoffset, activeupondischarge, diagnosisoffset, diagnosispriority, hospitaladmitoffset).

Table A1. Preprocessing Features.

Feature	Table	Description
patientUnitStayID	patient	A distinct ICU admission. The same patient can have multiple.
observationOffset	vital periodic	The number of minutes, since admission, before the periodic value was recorded.
diagnosisoffset	diagnosis	Number of minutes, since admission, before diagnosis was recorded.
diagnosisPriority	diagnosis	Diagnosis was marked as Primary, Major, or Other
diagnosisString	diagnosis	The full pathstring of diagnosis selected in Philips eCareManager software with sections separated with pipes (e.g: cardiovascular | shock/hypotension | sepsis)
ICD9Code	diagnosis	International Classification of Diseases code used to classify diagnoses (e.g: 518.81, 491.20, etc.)

References

1. Weerasinghe, K.; Scahill, S.L.; Pauleen, D.J.; Taskin, N. Big data analytics for clinical decision-making: Understanding health sector perceptions of policy and practice. *Technological Forecasting and Social Change* **2022**, *174*, 121222.
2. Rajkomar, A.; Oren, E.; Chen, K.; Dai, A.M.; Hajaj, N.; Hardt, M.; Liu, P.J.; Liu, X.; Marcus, J.; Sun, M.; others. Scalable and accurate deep learning with electronic health records. *NPJ digital medicine* **2018**, *1*, 1–10.
3. Rudin, C.; Chen, C.; Chen, Z.; Huang, H.; Semenova, L.; Zhong, C. Interpretable machine learning: Fundamental principles and 10 grand challenges. *Statistic Surveys* **2022**, *16*, 1–85.
4. Raghupathi, W.; Raghupathi, V. Big data analytics in healthcare: promise and potential. *Health information science and systems* **2014**, *2*, 1–10.
5. Nguyen, T.; Diakiw, S.; VerMilyea, M.; Dinsmore, A.; Perugini, M.; Perugini, D.; Hall, J. Efficient automated error detection in medical data using deep-learning and label-clustering. *Scientific reports* **2023**, *13*, 19587.
6. Rudin, C. Stop explaining black box machine learning models for high stakes decisions and use interpretable models instead. *Nature machine intelligence* **2019**, *1*, 206–215.
7. Mehrabi, N.; Morstatter, F.; Saxena, N.; Lerman, K.; Galstyan, A. A survey on bias and fairness in machine learning. *ACM computing surveys (CSUR)* **2021**, *54*, 1–35.
8. Amann, J.; Blasimme, A.; Vayena, E.; Frey, D.; Madai, V.I.; Consortium, P. Explainability for artificial intelligence in healthcare: a multidisciplinary perspective. *BMC medical informatics and decision making* **2020**, *20*, 1–9.
9. Sun, Y.; Wong, A.K.; Kamel, M.S. Classification of imbalanced data: A review. *International journal of pattern recognition and artificial intelligence* **2009**, *23*, 687–719.
10. Wong, A.K.; Zhou, P.Y.; Butt, Z.A. Pattern discovery and disentanglement on relational datasets. *Scientific reports* **2021**, *11*, 5688.
11. Wong, A.K.; Zhou, P.Y.; Lee, A.E.S. Theory and rationale of interpretable all-in-one pattern discovery and disentanglement system. *npj Digital Medicine* **2023**, *6*, 92.
12. Northcutt, C.G.; Athalye, A.; Mueller, J. Pervasive label errors in test sets destabilize machine learning benchmarks. *arXiv preprint arXiv:2103.14749* **2021**.

13. Zhou, Z.H. *Ensemble methods: foundations and algorithms*; CRC press, 2012.
14. Khan, A.A.; Chaudhari, O.; Chandra, R. A review of ensemble learning and data augmentation models for class imbalanced problems: Combination, implementation and evaluation. *Expert Systems with Applications* **2023**, p. 122778.
15. Pollard, T.J.; Johnson, A.E.; Raffa, J.D.; Celi, L.A.; Mark, R.G.; Badawi, O. The eICU Collaborative Research Database, a freely available multi-center database for critical care research. *Scientific data* **2018**, *5*, 1–13.
16. Parmar, S.; Shan, T.; Lee, S.; Kim, Y.; Kim, J.Y. Extending Machine Learning-Based Early Sepsis Detection to Different Demographics. 2024 IEEE First International Conference on Artificial Intelligence for Medicine, Health and Care (AIMHC). IEEE, 2024, pp. 70–71.
17. Singer, M.; Deutschman, C.S.; Seymour, C.W.; Shankar-Hari, M.; Annane, D.; Bauer, M.; Bellomo, R.; Bernard, G.R.; Chiche, J.D.; Coopersmith, C.M.; others. The third international consensus definitions for sepsis and septic shock (Sepsis-3). *Jama* **2016**, *315*, 801–810.
18. Hilarius, K.W.; Skippen, P.W.; Kissoon, N. Early recognition and emergency treatment of sepsis and septic shock in children. *Pediatric Emergency Care* **2020**, *36*, 101–106.
19. Dellinger, R.P.; Levy, M.M.; Rhodes, A.; Annane, D.; Gerlach, H.; Opal, S.M.; Sevransky, J.E.; Sprung, C.L.; Douglas, I.S.; Jaeschke, R.; others. Surviving sepsis campaign: international guidelines for management of severe sepsis and septic shock: 2012. *Critical care medicine* **2013**, *41*, 580–637.
20. Pedregosa, F.; Varoquaux, G.; Gramfort, A.; Michel, V.; Thirion, B.; Grisel, O.; Blondel, M.; Prettenhofer, P.; Weiss, R.; Dubourg, V.; others. Scikit-learn: Machine learning in Python. *the Journal of machine Learning research* **2011**, *12*, 2825–2830.
21. Haixiang, G.; Yijing, L.; Shang, J.; Mingyun, G.; Yuanyue, H.; Bing, G. Learning from class-imbalanced data: Review of methods and applications. *Expert systems with applications* **2017**, *73*, 220–239.
22. Palczewska, A.; Palczewski, J.; Marchese Robinson, R.; Neagu, D. Interpreting random forest classification models using a feature contribution method. *Integration of reusable systems* **2014**, pp. 193–218.
23. Marchenko, O.; Russek-Cohen, E.; Levenson, M.; Zink, R.C.; Krukas-Hampel, M.R.; Jiang, Q. Sources of safety data and statistical strategies for design and analysis: real world insights. *Therapeutic Innovation & Regulatory Science* **2018**, *52*, 170–186.

Disclaimer/Publisher's Note: The statements, opinions and data contained in all publications are solely those of the individual author(s) and contributor(s) and not of MDPI and/or the editor(s). MDPI and/or the editor(s) disclaim responsibility for any injury to people or property resulting from any ideas, methods, instructions or products referred to in the content.